Journal of Aerosol Science 67 (2014) 104–118

Contents lists available at ScienceDirect

Journal of Aerosol Science

journal homepage: www.elsevier.com/locate/jaerosci

Improved particle scavenging by a combination of ultrasonics and water sprays

W. Ran [a], J.R. Saylor [a,*], R.G. Holt [b]

[a] Clemson University, Department of Mechanical Engineering, Clemson, SC 29634, USA
[b] Boston University, Department of Mechanical Engineering, Boston, MA 02215, USA

ARTICLE INFO

Article history:
Received 23 May 2013
Received in revised form
15 August 2013
Accepted 16 August 2013
Available online 11 September 2013

Keywords:
Particles
Drops
Sprays
Scavenging
Ultrasonics

ABSTRACT

The results of an experimental study are presented where an ultrasonic field was used to increase the scavenging of micron-scale particles by water sprays. Specifically, an ultrasonic standing wave field was set up between an ultrasonic transducer and a reflector, creating multiple pressure nodes. These nodes are locations where drops collect into what we call accretion disks. Significant increases in the scavenging coefficient were observed when these accretions disks were present. Experiments conducted in the presence of an ultrasonic standing wave field and a water spray yielded scavenging coefficients as large as 140% of those which were obtained using a spray alone. Also, experiments conducted with the ultrasonic field present, but detuned so that accretion disks did not form, showed no significant improvement over the case without ultrasonics at all. The scavenging coefficients are presented as a function of particle diameter and water flow rate.

1. Introduction

This work focuses on the use of water sprays to remove particles from a particle laden stream of air. This is a common situation encountered, for example, when particles are removed from a polluted air stream, such as a smokestack, using wet scrubbers, or in environments such as mines where sprays are used to reduce the high levels of coal dust or silica dust which renders the air dangerous to human health and can make the air explosive. Particulate pollutants negatively impact the health of humans in several ways, including increases in mortality in individuals with pre-existing lung conditions (Davis et al., 2002; Schwartz, 1994) via increased cardiovascular disease morbidity and mortality (Johnson, 2004; Pope et al., 2004; Suwa et al., 2002; Verrier et al., 2002), and via increased prevalence or exacerbation of lung ailments such as lung cancer (Cohen, 2000; Pope et al., 1995, 2002), chronic obstructive pulmonary disease (COPD) (Schikowski et al., 2005) and asthma (Docker & Pope, 1994; Schwartz et al., 1993; Seaton et al., 1995), among others. Studies of city populations show increases in mortality on days when particulate pollution levels are elevated (Schwartz & Dockery, 1992; Schwartz et al., 2002). In the mining industry, exposure to silica dust causes silicosis, and exposure to coal dust results in coal workers' pneumoconiosis (CWP) also known as black lung disease, diseases that continue to kill mine workers. The increased use of diesel engines in mines has raised concerns over exposure of mine workers to diesel particulate matter, presenting yet another potential threat to human health from particulate pollutants (NIOSH, 2002).

Sprays are commonly used to remove particles from air. This is the case, as noted above, in the use of wet scrubbers in smokestacks. Sprays are ubiquitous in the mining environment where they are used to prevent particles from entering the

* Corresponding author. Tel.: +1 864 656 5621; fax: +1 864 656 4435.
E-mail address: jsaylor@clemson.edu (J.R. Saylor).
URL: http://myweb.clemson.edu/~jsaylor/ (J.R. Saylor).

0021-8502/$ - see front matter © 2013 Elsevier Ltd. All rights reserved.
http://dx.doi.org/10.1016/j.jaerosci.2013.08.009

air, and also to reduce their levels once they have entered the air. Because sprays are used so often in particle scavenging, increasing their ability to scavenge particles would have a significant impact.

The ability of a drop or group of drops, such as a spray, to capture particles can be quantified by the scavenging coefficient:

$$E = \frac{n_s}{n_T} \times 100\% \tag{1}$$

where n_s is the number of particles scavenged by the drop (or collection of drops) and n_T is the total number of particles within the cylindrical volume swept out by the drop(s) as it travels through the particle laden air stream. The scavenging coefficient E is dependent on the complicated physics of particle–drop interactions, and is affected by many factors. These include the drop and particle densities, the diameters of the drop and particle, the charge on the drop and particle, the physical properties of the liquid such as surface tension and viscosity, and the airflow characteristics around the drop.

For a given drop diameter D, E is sensitively dependent on the particle diameter d. Specifically, plots of E versus d reveal a minimum in E which can be quite low. This minimum is the result of two competing trends. At large particle diameters, inertia plays a large role in particle scavenging since the particle, unable to follow the streamlines around the drop, impacts the drop. At very small particle diameters these inertial effects do not play a role, but Brownian motion enables a relatively large fraction of particles in the boundary layer near the drop to diffuse[1] toward the drop and thereby impact the drop in that fashion. These diffusive effects increase with decreasing d, while inertial effects increase with increasing d. Accordingly, there is a range of particle diameters that falls between the inertially-dominant and diffusive-dominant regimes where neither inertial or diffusive processes are effective, and where values of E are relatively low. This region where a minimum in E is observed is often referred to as the "Greenfield gap", after Greenfield who analytically investigated the scavenging coefficients of particles in rainfall and was first to show the existence of this minimum (Greenfield, 1957). Significant research on rain/particle interactions has taken place since the time of Greenfield, excellent examples of which can be found in the work of Beard and co-workers, such as Beard & Grover (1974) and Beard (1974). A plot taken from Greenfield's paper is presented in Fig. 1 which shows reduced E for particle diameters ranging from ~ 0.1 μm to ~ 1.0 μm. This range will differ depending on the characteristics of the drop, the particle, and the airflow, among other factors. However, for applications relevant to the current work where water drops have diameters ranging from several tens of microns to a millimeter, the gap in scavenging coefficient corresponds roughly to that shown in Fig. 1. This was shown, for example, by Pranesha & Kamra (1996) who compiled the work of several authors, incorporating water drops where D ranged from 87 μm to 4.8 mm and particle densities ranged from 1000 kg/m^3 to 2500 kg/m^3. Although the location of the scavenging gap varied with experimental conditions, the minimum in E resided between 0.1 μm and 1.0 μm, with few exceptions.

The existence of a minimum in E for particle diameters, $d = 0.1$–1.0 μm is of particular concern for pulmonary illness. Alveolar deposition of particles peaks for d slightly larger than 1 μm, and significant alveolar deposition occurs for particles ranging in diameter from 0.01 μm to 10 μm (EPA, 1999; Heyder et al., 1986). Particles with $d < 2.5$ μm (often referred to as PM2.5) are believed to pose the greatest health risk (Schwartz et al., 2002). This means that the range in d that presents the greatest threat to pulmonary health overlaps the range in d where sprays are least effective in removing particles from air. Because sprays are used in the wet scrubbers of smokestacks and in particle control in mines, a method that could improve the scavenging coefficient of spray drops for particle diameters in the 0.1–1.0 μm range could lead to technologies that would significantly improve pulmonary health.

The goal of the work presented herein was to determine if ultrasonics could be used to improve the ability of sprays to scavenge micron-scale particles. Our hypothesis was that ultrasonics could be used in such a way that micron scale particles would be forced into contact with spray drops. Such an approach is theoretically possible, since a force is experienced by any object that scatters acoustic[2] waves in a medium, e.g. particles or drops. This acoustic radiation force F_{ar} has often been used to levitate objects in a standing wave field, a technique that has found application in many areas ranging from the study of fluid mechanics (Marston & Thiessen, 2004; Shi et al., 1995; Trinh et al., 1996) to containerless processing of materials (Weber et al., 1994) as well as in analytical chemistry applications (Santesson & Nilsson, 2004). In a typical application, acoustic levitation is achieved by placing an ultrasonic transducer oriented in the vertical direction, directly beneath a reflector (typically a flat metal disk), with the two separated by an integer number of half wavelengths to create a standing wave field. The acoustic radiation force should act to move particles and drops toward the nodes or anti-nodes (depending on the properties of the particles/drops and the ambient fluid) of the standing wave field (Crum, 1971; Marston & Thiessen, 2004).

An example of such a setup is presented in Fig. 2, which shows an ultrasonic transducer (below) and a reflector (above). A fine water spray has been introduced into the general vicinity of the field by a nebulizer (the tube on the upper left hand side of the image), and the fine spray drops have accumulated in the pressure nodes, forming what we call "accretion disks". In the center of these disks, enough drops have agglomerated with each other to form relatively large drops. In the figure, these large drops in the center of the accretion disk have a weight less than the acoustic radiation force. However, as time

[1] Here we are modeling Brownian motion as diffusion.

[2] Herein the words "acoustic" and "ultrasonic" are used interchangeably, though any practical device would have to use ultrasonics due to the auditory damage that would result should audible frequencies be employed.

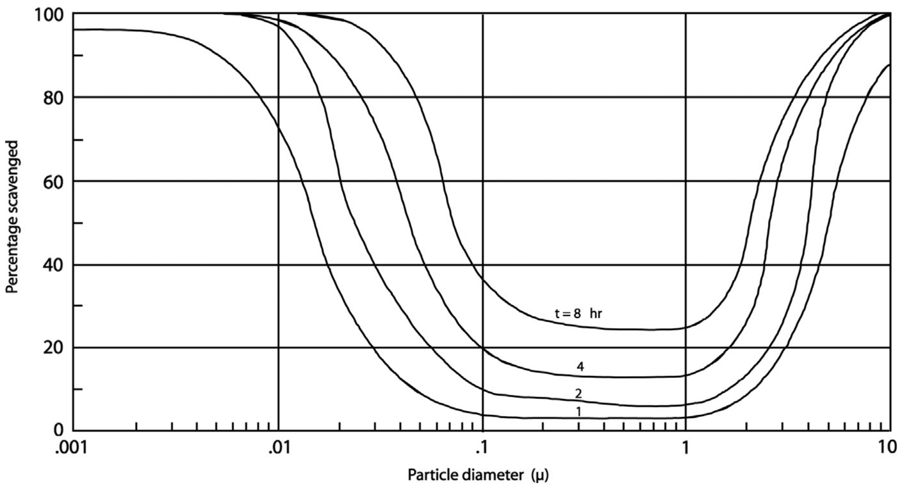

Fig. 1. Plot of scavenging coefficient versus particle diameter for particles in rain. Plot due to Greenfield (1957). (c) American Meteorological Society. Used with permission.

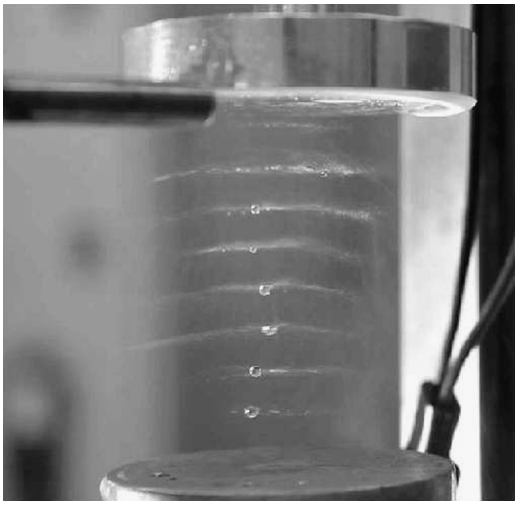

Fig. 2. Image showing droplets accumulated in the pressure nodes of an ultrasonic standing wave field to create accretion disks.

passes, continuous introduction of the fine spray drops increases the size of these large drops, and eventually the drop weight exceeds F_{ar}, causing them to fall. As noted above, the hypothesis that drove the present work is that micron-scale particles introduced in a setup, like that shown in Fig. 2, would be more effectively scavenged by the spray due to the presence of the ultrasonic standing wave field. The rationale behind this hypothesis is that just as F_{ar} causes fine water droplets in Fig. 2 to accumulate in the nodes, so too should it cause particles to migrate to these nodes. This accumulation of particles would increase the chance that particles would (a) combine with the fine water drops, (b) combine with the large drop in the center of the accretion disks, and/or (c) combine with each other. Any or all of these effects would increase particle scavenging. The goal of the present paper was to ascertain if an ultrasonic standing wave field could cause an increase in scavenging by a water spray and, if possible, to determine which combination of the above three mechanisms was responsible for that increase, if it exists. The experimental method designed to achieve these goals is now described.

2. Experimental method

The overall approach in this work was to build a small scale scrubber and determine E for that scrubber with and without an ultrasonic standing wave field. This scrubber consisted of, essentially, a small box wherein the ultrasonic field could be established, and where a fine water spray and a flow of particle laden air could be introduced. A horizontally oriented ultrasonic standing wave field was established inside the scrubber, and experiments were conducted with and without the field. This apparatus is described in greater detail, below.

2.1. Experimental setup

The entire test facility is shown in Fig. 3. The heart of this facility is the scavenging chamber (the dashed box in Fig. 3) which is illustrated by itself in Fig. 4, and is the location where scavenging actually occurs. The scavenging chamber is rectangular with a volume of 370 cm^3. A detailed schematic of this chamber along with its dimensions is presented in Fig. 5.

A nebulizer was mounted on the top of the chamber, and directed downward to create a fine water spray having an arithmetic mean diameter of 92 μm with a standard deviation of 111 μm. The method for measuring the drop diameter is presented later in this section. The nebulizer uses ultrasonic energy to generate the fine water mist, which was initially a point of concern due to possible interactions with the ultrasonic standing wave field created by the transducer. However, preliminary experiments revealed that this was not the case. Specifically, a vibration sensor was inserted into the ultrasonic standing wave field; the output of this sensor showed that the sound pressure generated by the nebulizer was negligible compared to that of the standing wave in the scavenging chamber.

The water flow rate that was run through the nebulizer ranged from $Q=10$ to 90 ml/min in these experiments, and was precisely controlled using a peristaltic pump. A water drain was located at the bottom of the chamber to drain accumulated water; this water contained the scavenged particles.

As shown in Figs. 4 and 5, particle laden air was introduced via a port at one side of the top of the scavenging chamber. The air flow then exited the chamber through a similar port located at the other side of the top of the chamber. Clearly other flow configurations could have been chosen, and a different configuration may result in results different from those reported here. Indeed, an excellent follow-on study would be a parametric study of the flow in the chamber designed to optimize scavenging. However, as no study of this type has been attempted heretofore, our choice for the inlet and exit locations of the particle laden air was driven primarily by common sense. As shown in Fig. 4, both the spray inlet and the particle laden air inlet were located at the top of the chamber and directed downward. This configuration imparted downward momentum to the flow. By having the air flow exit also at the top of the chamber, the flow (both the particle laden air, and the spray) was forced to travel downward into the chamber and then turn back around to exit at the top. It was thought that this would maximize the amount of time that the spray and particle interacted but, again, other choices might be better.

The standing wave field was established in the scavenging chamber using a previously developed ultrasonic transducer and reflector plate combination separated by 28 cm. As shown in Fig. 4, the acoustic wave emanating from the transducer passed through a plexiglass tube having a diameter of 5 cm, which entered the main portion of the scavenging chamber via

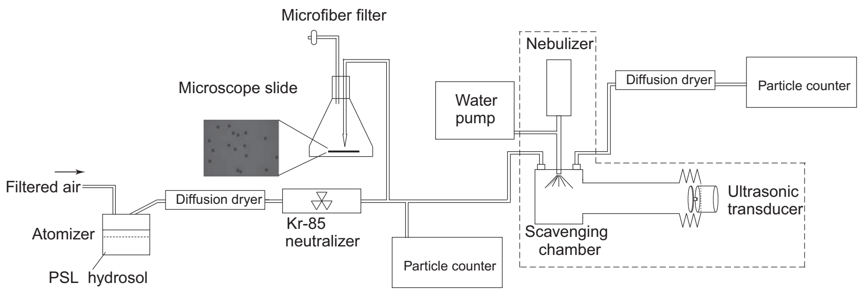

Fig. 3. Experimental apparatus.

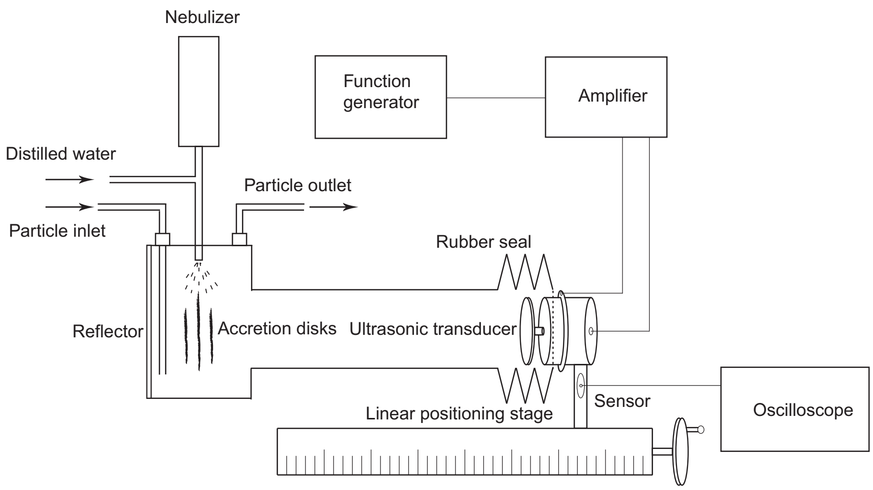

Fig. 4. Scavenging chamber with affiliated equipment (expanded view of the dashed box in Fig. 3).

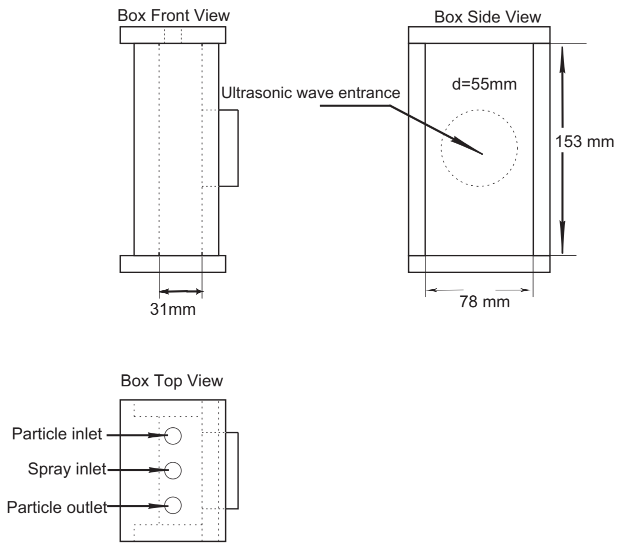

Fig. 5. Detailed view of the scavenging chamber. The dimensions of this chamber are 153 mm × 78 mm × 31 mm.

an air tight hole. This approach provided a clear path from the transducer to the reflector. Recessing the transducer away from the path of the spray ensured that the transducer did not get wet, which was an important factor. Preliminary experiments used a different setup where the transducer was not recessed from the main portion of the chamber. During these experiments the transducer became wet and would re-atomize the drops that landed on the transducer surface. Hence, drops which had already scavenged particles would subsequently be re-atomized, reintroducing scavenged particles back into the air. The recessed transducer approach illustrated in Fig. 4 avoided this problem. The scavenging chamber was airtight except for the particle inlet and outlet. A water drain (not illustrated) was also open to atmospheric pressure, however a layer of water was always present at the bottom of the chamber, preventing ambient air from entering.

One set of particles investigated here was polystyrene latex (PSL) microspheres having diameters of 0.7, 0.9, 2.3, 3.1, and 4.2 μm. PSL was selected for several reasons. First, these particles are easily procured in highly monodisperse distributions. Hence, by atomizing solutions of these spheres, a monodisperse distribution can be formed as long as the water is completely evaporated and as long as the atomized drops had only one PSL sphere per drop. Secondly, the alternative approach of atomizing solutions of soluble salts such as sodium chloride or disodium fluorescein created potential problems in high humidity environments where phase transformation and growth can occur (Tang, 1976) and indeed did occur during preliminary work where we attempted this approach.

To create a monodisperse distribution of PSL in air, a PSL hydrosol supplied by Spherotech Inc. was first diluted using distilled water. After dilution the particles were washed several times using a centrifuge. During this process, the water/particle solution was centrifuged, forcing the PSL particles to the bottom of the container after which the water residing above the particle layer was easily decanted. This process was repeated several times, thereby removing impurities. Finally, the resulting hydrosol was sonicated to disperse agglomerated PSL particles. A TSI model 9302 atomizer was used to atomize the diluted hydrosol into a mist which was convected through the experimental apparatus via a flow of clean dry air (labeled “filtered air” in Fig. 3) at a flow rate of 12 l/min. The dry air partially evaporated the water drops containing the PSL spheres. To ensure that the particles were fully dried, the flow was passed through a diffusion dryer (also illustrated in Fig. 3) to remove any remaining moisture.

PSL aerosols formed using this method have been shown to contain significant static charge (Whitby & Liu, 1968). To eliminate any potential charging problems, a TSI model 3012 neutralizer was used, which consisted of a 74 MBq Kr-85 radioactive source. This source was placed in line with the flow, downstream of the diffusion dryer.

To measure the particle size distribution (PSD), particle samples were collected by directing a portion of the airflow just downstream of the neutralizer onto a glass microscope slide. This was done via a tee fitting which directed part of the airflow away from the remainder of the experimental facility and into an Erlenmeyer flask which had a clean microscope slide located at its bottom. The microscope slide was exposed to the flow of particles during the entire course of an experimental run (typically $\sim$5 h). Images of particles were then obtained using a Leica (DM750) microscope fitted with a digital camera that was used to acquire images at 100 different locations on each microscope slide with appropriate magnification for the particle diameter being considered. A separate image of a ruler was also obtained and used to generate the micron/pixel conversion necessary to obtain particle diameters from the digital images. The resulting conversion factor varied from 0.02 μm/pixel to 0.05 μm/pixel. The number of particles imaged for each experiment ranged from 2000 to 4000, depending on the magnification and the areal deposition density on the slide. An image processing sequence was developed to obtain particle diameters from the particle images that began with Otsu's (1979) algorithm which converted

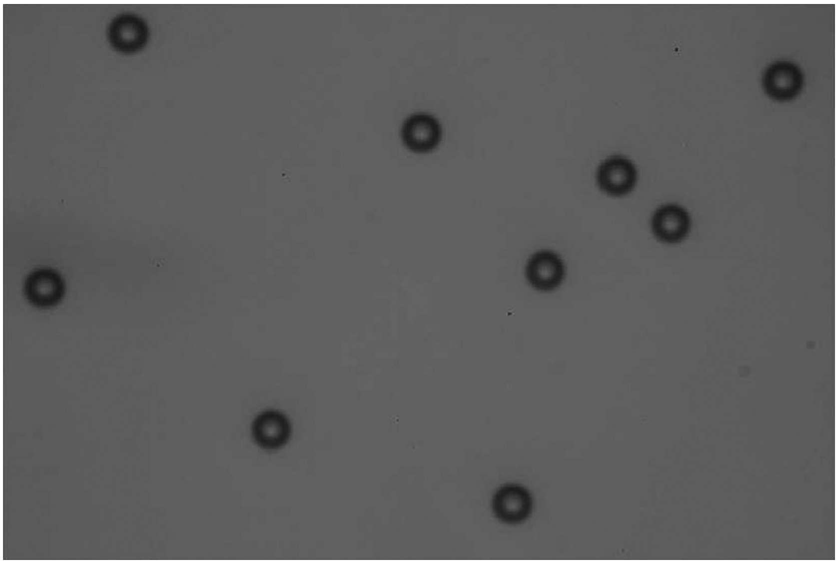

Fig. 6. Sample image obtained for PSL particles deposited on a microscope slide. This image is not processed.

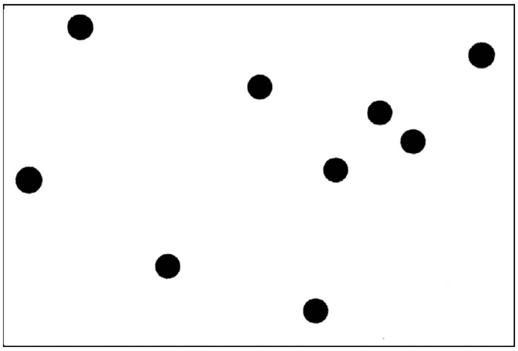

Fig. 7. Binary version of the image presented in Fig. 6. This image was obtained by applying the image processing algorithm described in the text.

the grayscale images to binary images. Each image was then segmented into separate particles based on the connectivity of each pixel. The area of each particle was then obtained by summing all of the connected pixels. This area was converted to a diameter, assuming that each particle was spherical. A roundness criterion was also developed to enable rejection of the rare dust particle. A sample grayscale image of deposited particles is presented in Fig. 6, and the binary version of this image obtained using the aforementioned image processing steps is presented in Fig. 7.

As noted above, PSL particles having five different diameters were investigated. According to the manufacturer, the average diameter for these were 0.7, 0.92, 1.7, 2.78, and 3.8 μm. The PSDs obtained using the method described above are presented in Fig. 8 where f is plotted against d for each of the five particle solutions used. Here, the probability f of observing a particle of a specific diameter is defined as

$$f = \frac{n}{N\Delta d} \tag{2}$$

where n is the number of particles in a given size bin, N is the total number of particles in all bins and Δd is the bin width. The average diameter and standard deviation obtained from the data presented in Fig. 8 are the following: 0.7 ± 0.1, 0.9 ± 0.2, 2.3 ± 0.4, 3.1 ± 0.4, 4.2 ± 1.5 μm. There is no evidence of doublets or triplets in these distributions, suggesting that the variation is due to variability in the actual particles, and not agglomeration during the atomization process. The difference between the average diameter provided by the manufacturer and the value measured here is most likely due to settling of the larger particles to the bottom of the container where the inlet to the atomizer is located. This could explain the slightly larger average diameter measured here, compared to the manufacturer's quoted value. The fact that the measured diameters are larger for all but the two smallest particle sizes where less settling would be expected supports this conclusion.

The second set of particles used in these experiments was those present in the ambient air of the laboratory. While these experiments were much less controlled than for the PSL case, it seemed a worthy set of experiments to conduct due to the

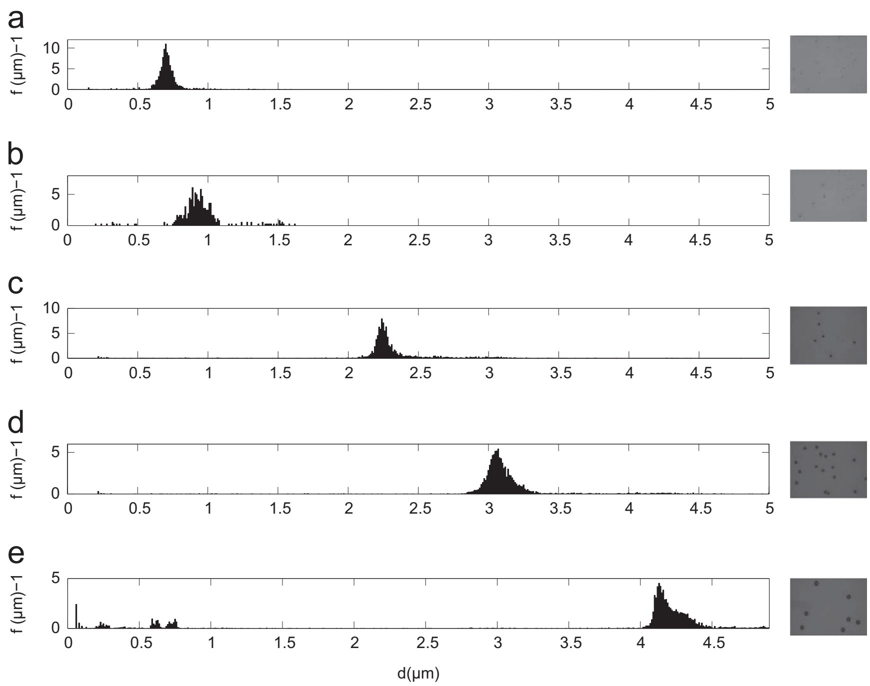

Fig. 8. Particle size distributions for the five particle solutions used. (a) 0.7 ± 0.1 μm. (b) 0.9 ± 0.2 μm. (c) 2.3 ± 0.4 μm. (d) 3.1 ± 0.4 μm. (e) 4.2 ± 1.5 μm. A sample grayscale image obtained using the microscope is included to the right of each distribution.

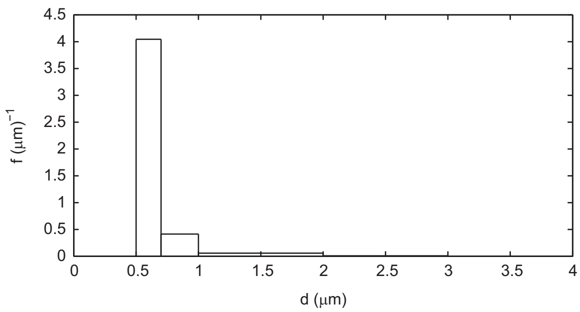

Fig. 9. Particle size distribution for ambient air particles in the laboratory. The average particle diameter is $d = 0.8$ μm.

ease of access to this particle source. The distribution of particle diameters for this ambient air case is presented in Fig. 9, which has less resolution in d than for the PSL case presented in Fig. 8. This is because the ambient air particles were sized using a particle counter (Met One, Hach Ultra Analytics Inc.) having only six size bins, as opposed to the microscope imaging system used in obtaining Fig. 8. The microscope imaging method used for the PSL particles was not used for the ambient air particles since there was no method that could be used to discriminate particles from noise.

The size distribution of the droplets generated by the nebulizer was obtained by nebulizing a solution of disodium fluorescein salt having a known concentration. The resulting droplets were dried in a heated plastic column leaving solid fluorescein salt particles. The size distribution of these particles was then obtained using the same microscope method used in obtaining the PSL distributions. The original drop diameter size distribution was then extracted using the measured particle diameter and the fluorescein salt concentration.

The ultrasonic transducer used in these experiments was a half-wave resonator based on the full-wave design of Trinh (1985) and is illustrated in Fig. 10. As shown in the figure, two aluminum disks were used to sandwich two piezoelectric lead–zirconate–titanate (PZT) disks. These disks were separated from each other by a thin copper disk, which served as one electrode, with the body of the aluminum transducer serving as the other. Using the dimensions presented in Fig. 10, this transducer has a resonant frequency of $f_r \sim 30$ kHz. Prior to each experiment the system was tuned by attaching a piezoelectric sensor to the back of the transducer, and adjusting the frequency applied to the transducer from a nominal initial setting of 30 kHz until a maximum was observed in the signal amplitude from the sensor, indicating that f_r had been attained. Once f_r was attained, the distance between the transducer and the reflector plate h was tuned so that this distance

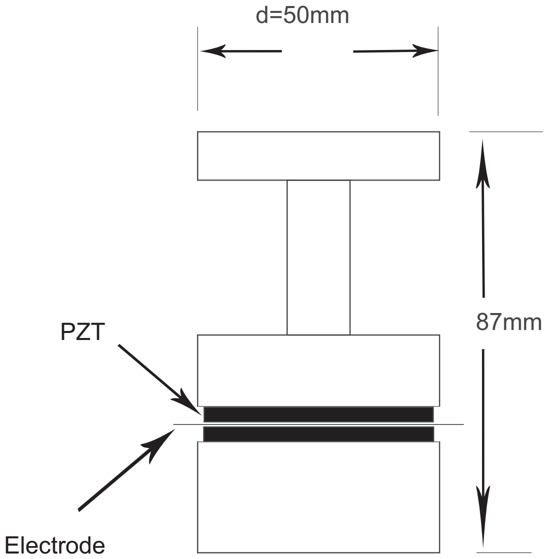

Fig. 10. Schematic of the ultrasonic transducer used in these experiments.

was an integer number of half wavelengths, i.e.

$$h = \frac{n\lambda}{2} \tag{3}$$

where λ is the acoustic wave length obtained from:

$$\lambda = \frac{c}{f} \tag{4}$$

where c is the sound speed. As shown in Fig. 4, the transducer was mounted on a linear positioning stage (Velmex, A60) allowing for the adjustment of h. As a first approximation, h was obtained from Eqs. (3) and (4). This value is imprecise since the local sound speed c is a necessarily estimated value based on the lab temperature and pressure which cannot be known exactly in the air space between the transducer and the reflector. Accordingly, h was tuned by turning on the water spray and adjusting h until the fine water drops accumulated in the pressure nodes instead of falling straight down, showing that a standing wave field had been attained and Eq. (3) had been satisfied. An image is presented in Fig. 2 showing this accumulation of spray drops in the nodes. A voltage of 90 VAC was applied to the transducer. Higher voltages caused the transducer to overheat and become unstable.

Two identical Met One 237A particle counters (Hach Ultra Analytics Inc.) were used to measure the concentration of particles upstream and downstream of the scavenging chamber, as shown in Fig. 3. The particle counters are capable of detecting particles larger than 0.5 μm. Preliminary tests showed that for a PSL aerosol source, if the sampling tube lengths were equal for both counters, there was less than a 1% difference between the readings of the two particle counters. Because the particle counters are capable of detecting particles and water droplets, a diffusion dryer was placed between the scavenging chamber and the downstream particle counter to eliminate any liquid water from the flow, thereby ensuring that droplets were not sampled by the counter. For particles smaller than 1 μm there was negligible particle loss to the diffusion dryer. For particles larger than 1 μm, particle loss to the diffusion dryer was less than 20%. As will be demonstrated below, this loss is accounted for and does not affect measurements of E. The sampling rate for both particle counters was set to 5 s/sample. Sampling from the two particle counters was synchronized to allow a simultaneous comparison of the particle concentration at the upstream and downstream locations, ensuring that measurement of E was not affected by drift in the particle generation rate or drift in any other facet of the system.

2.2. Experimental procedure

Before each experiment, clean air was passed through the system until both particle counters read zero. The air flow used in this experiment was obtained from the laboratory air compressor and was filtered by a 0.3 μm cutoff filter. Once the particle counters read zero, the spray (ultrasonic nebulizer) was turned on, and the downstream particle counter was monitored for 5 min to ensure that it remained at zero, thereby ensuring that droplets were evaporating completely prior to reaching that counter. Then the spray was turned off and the aerosol generator (the TSI atomizer) was turned on, and was allowed to run until both particle counters read a constant, stable value. Once this was achieved, particle concentration data acquisition began.

During data acquisition, the apparatus was operated in one of two modes. One mode was deposition mode, where the water spray and the ultrasonic transducer were both off. In this mode, any differences between the upstream and downstream particle counters is due solely to particle deposition in the lines (tube wall, diffusion dryer, etc.). The second mode was scavenging + deposition mode during which the water spray was turned on. In scavenging + deposition mode, the difference between the upstream and downstream particle counter readings is due to the combined effect of particle deposition in the lines and particle scavenging by the spray. Scavenging + deposition mode was run with and without energizing the ultrasonic transducer. During an experiment, these two modes were operated sequentially, each for 6 min, switching back and forth between the modes until the data storage buffers in the particle counters were full, which was typically 36 min. Once this occurred, the data was downloaded to a computer for subsequent analysis. This procedure was performed five times for each run, resulting in a total of 180 min for actual acquisition of data. Including the preliminary procedures prior to data-taking, each run took approximately 5 h. This procedure was the same for experiments with or without the ultrasonics turned on.

A sample time trace is presented in Fig. 11(a) showing the particle concentrations of the upstream particle counter C_u and the downstream particle counter C_d. The percent of particles lost L is computed according to the equation:

$$L = \frac{C_u - C_d}{C_u} \times 100\% \tag{5}$$

Figure 11(b) is a plot of L obtained by applying Eq. (5) to the data of Fig. 11(a).

Figure 11(a) shows that there is significant particle loss due to the deposition of particles. In order to isolate the effect of the spray alone (and not the deposition), we compute E for the chamber as

$$E = L_2 - L_1 \tag{6}$$

where the subscripts 1 and 2 in Eq. (6) refer to the deposition mode and the scavenging + deposition mode, respectively. By computing E in this way, the effect of particle deposition in the walls and lines of the system is eliminated. That Eq. (6) is

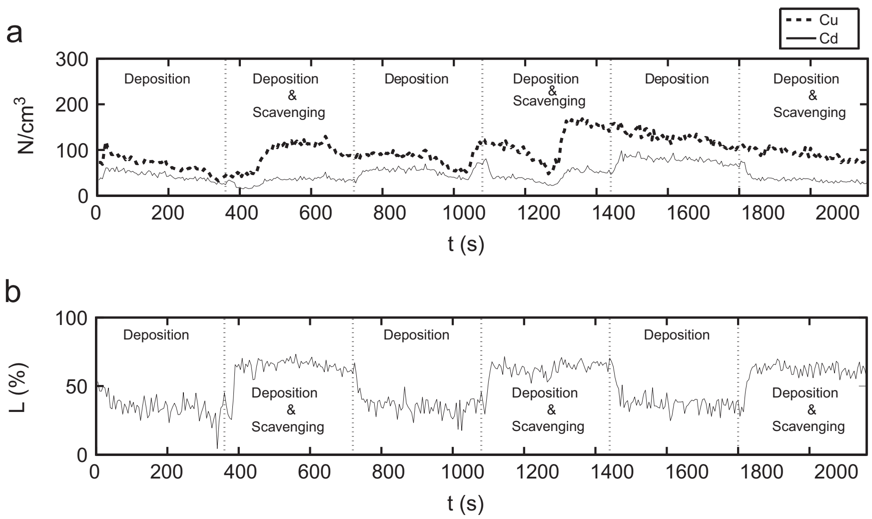

Fig. 11. (a) Particle concentration time traces for the upstream C_u and downstream C_d particle counters, obtained from a sample experiment. (b) The time trace of L obtained by applying Eq. (5) to the data in (a).

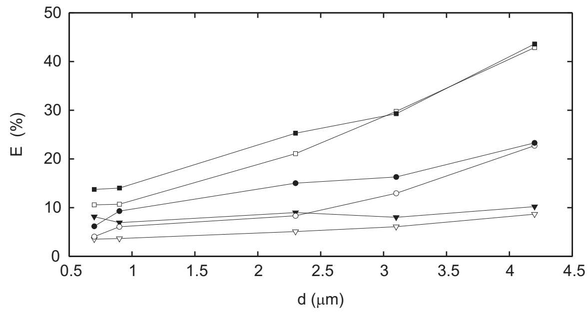

Fig. 12. Plot of the scavenging coefficient E versus particle diameter d for experiments using PSL spheres. Data is presented for three different water flow rates (▿: Q=0.43 ml/s; ○: Q=0.87 ml/s; □ : Q=1.23 ml/s). Open symbols represent runs without an ultrasonic standing wave field, and filled symbols represent runs with an ultrasonic standing wave field.

the same as Eq. (1) can be seen by substituting Eq. (5) into Eq. (6) to give (ignoring the factor of 100 for simplicity):

$$E = \frac{C_{u2} - C_{d2}}{C_{u2}} - \frac{C_{u1} - C_{d1}}{C_{u1}} \quad (7)$$

which is the fraction of the incoming particles removed due to both scavenging and deposition, minus the fraction of the incoming particles removed due to just deposition. This difference is the fraction of the incoming particles removed due to scavenging, viz., the scavenging coefficient for the entire chamber, E.

3. Results

The main results of this work are presented in Fig. 12 where the scavenging coefficient E is plotted against the particle diameter d for the case where PSL spheres were used. The particle diameter plotted in this figure is the average diameter, and the distribution for each of these diameters is presented in Fig. 8. Each scavenging coefficient plotted in Fig. 12 is the average scavenging coefficient calculated by Eq. (6) based on 1800 particle concentration samples taken in an experiment that lasted on the order of 5 h. The 95% confidence intervals for these scavenging coefficients are comparable in size to the symbols in Fig. 12 and are omitted for the sake of clarity in this particular figure where the largest 95% confidence interval was 1.2%. The air flow rate was 12 l/min for all experiments. For each of the water spray flow rates, experiments are presented with and without the use of ultrasonics. Broadly speaking, Fig. 12 shows that E increases with particle diameter and flow rate. Also, this plot shows that the scavenging coefficient is increased by the presence of an ultrasonic standing wave field. This is not as clear as it could be in Fig. 12, and is better revealed in Fig. 13 where the percent improvement in scavenging, I is plotted against particle diameter, where I is defined as follows:

$$I = \frac{E_w - E_{wo}}{E_{wo}} \times 100\% \quad (8)$$

where E_w and E_{wo} are the scavenging coefficients with and without ultrasonics, respectively. Figure 13 shows that the percent improvement in E due to ultrasonics is significant, and approaches 150% when the water flow rate and particle diameter are small.

As noted earlier, in addition to using PSL particles, experiments were conducted using particles present in the ambient laboratory air. The difference in scavenging behavior for these two particle types is presented in Fig. 14. Specifically, E is plotted against the water flow rate for both particle cases. For the ambient air particles, the average diameter was 0.8 μm, and for the PSL particles the $d = 0.9$ μm case is plotted (the diameter closest to the ambient air particle diameter).

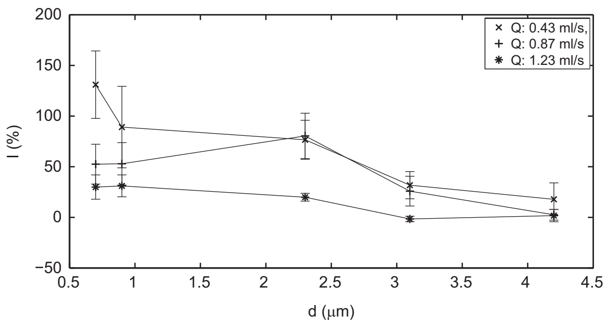

Fig. 13. Percent improvement in scavenging efficiency I due to ultrasonics versus particle diameter for the three water flow rates tested. The error bars are 95% confidence intervals.

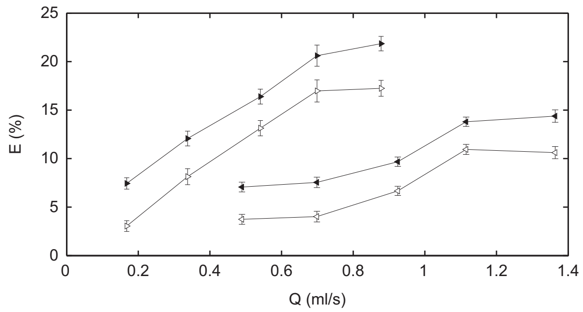

Fig. 14. Scavenging coefficient versus liquid flow rate. Comparison of the effect of ultrasonics on scavenging for ambient air particles (▹) and PSL particles (◃). Open symbols represent runs without an ultrasonic standing wave field and filled symbols represent runs with an ultrasonic standing wave field. The error bars are 95% confidence intervals.

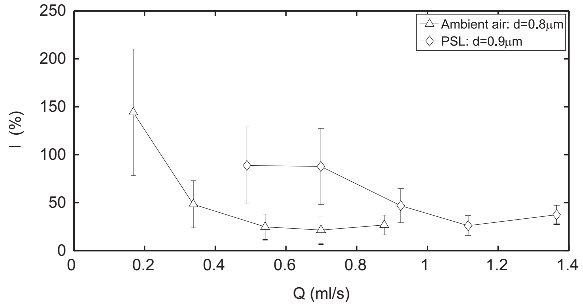

Fig. 15. Percent improvement in the scavenging coefficient due to the presence of an ultrasonic standing wave field plotted against the water flow rate Q. Data are presented for both PSL particles and ambient air particles. The error bars are 95% confidence intervals.

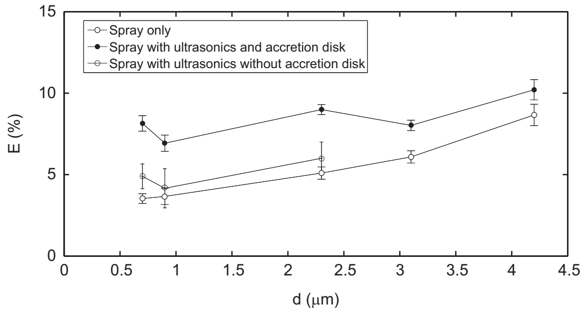

Fig. 16. Scavenging coefficient versus particle size. Comparison of the effect of the accretion disk on scavenging for PSL particles. The error bars are 95% confidence intervals.

In Fig. 14, the air flow rate is fixed at 12 l/min, while the liquid flow rate was varied from $Q=0.1$ ml/s to $Q=1.4$ ml/s. As was the case for Fig. 12, each point in Fig. 14 was obtained from 1800 particle concentration samples taken during a ~ 5 h experiment. We note that the PSL data presented in Fig 14 is also presented in Fig. 12, where the 95% confidence intervals were smaller than the symbol size. In Fig. 14, those 95% confidence intervals are larger than the symbol size (and therefore plotted) due to the difference in the scale of the y-axis in these two figures.

Figure 14 shows that at a fixed water spray flow rate, there is a significant increase in the scavenging coefficient in the presence of an ultrasonic standing wave field for both particle types. The percent improvement due to ultrasonics, I (Eq. (8)) is presented in Fig. 15, showing improvements approaching 150% for the ambient particles and approaching 100% for the 0.9 μm PSL particles. Though I is slightly larger for the PSL particles than for the ambient air particles at a given value of Q, further conclusions regarding the significance of the type of particle on I are difficult to make due to the difference in the average particle diameter for these two cases, the fact that the width of the size distributions of the two types of particle differs (see Figs. 8 and 9), as well as due to the large 95% confidence intervals for some of the points in Fig. 15.

To determine whether the increased scavenging due to the ultrasonic standing wave field is due to the accretion disks themselves, we ran experiments with the ultrasonic standing wave field in the usual way, and then with that field formed, but slightly detuned. The results are presented in Fig. 16 where E is plotted versus d for the case of the spray only, the spray with an ultrasonic standing wave field and the spray with a de-tuned ultrasonic standing wave field. The de-tuned field was attained by simply generating the field with the accretion disks as described in the Introduction, and then de-tuning the excitation field just to the point where the accretion disks seen in Fig. 2 were no longer visible. As the figure shows, the scavenging coefficients with the de-tuned field were not significantly better than for the case without any ultrasonic excitation at all, suggesting that the accretion disks are key to improved scavenging.

4. Discussion

The results presented in Figs. 12–16 clearly show that the presence of an ultrasonic standing wave field increases the scavenging of particles by a water spray. The results show that ultrasonic enhancement is most pronounced for particle sizes below about 2.5 μm, and for lower water flow rates. This was the main goal of this work. The other goal was to determine the mechanism of this increase. Specifically, it would be useful to determine if the increase is due to an increase in particles combining with each other, particles combining with small water drops, or particles combining with large drops. Here, we define small drops to be those created by the nebulizer (the fine water mist), and we define large drops as the millimeter-scale drops seen in the center of the accretion disks (Fig. 2). To address this question we first discuss the acoustic radiation force F_{ar} in detail.

The seminal work on F_{ar} dates back to King (1934), which was further developed by Hasegawa & Yosioka (1969) to address compressible particles. Gor'kov (1962) extended the theory to accommodate arbitrary acoustic fields. The aforementioned authors all invoked an inviscid fluid assumption, which is reasonable only when the particle diameter is much larger than the acoustic boundary layer:

$$\delta = \sqrt{\frac{2\nu}{\omega}} \tag{9}$$

where ν is the kinematic viscosity of the gas and ω is the angular frequency of the acoustic field. For the work presented above, d is on the order of one micron, and the ultrasonic frequency was 30 kHz, giving $\delta \sim 10\ \mu\text{m}$. Hence, the $d \gg \delta$ assumption is not valid for our work, requiring a theory which incorporates viscous effects. There are few of these, the most well-known being those due to Doinikov (1997), Danilov & Mironov (2000) and Settnes & Bruus (2012). Herein, we focus on the theory due to Settnes & Bruus (2012) since it is continuous in d, in contrast to the theories of Doinikov (1997) and Danilov & Mironov (2000). For a standing wave, Settnes & Bruus (2012) predict

$$F_{ar} = \frac{1}{2}\pi \Phi\left(\frac{\kappa_p}{\kappa_0}, \frac{\rho_p}{\rho_0}, \frac{2\delta}{d}\right) k E_{ac}\ \sin(2kz) d^3 \tag{10}$$

where

$$\Phi\left(\frac{\kappa_p}{\kappa_0}, \frac{\rho_p}{\rho_0}, \frac{2\delta}{d}\right) = \frac{1}{3} f_1\left(\frac{\kappa_p}{\kappa_0}\right) + \frac{1}{2} f_2\left(\frac{\rho_p}{\rho_0}, \frac{2\delta}{d}\right) \tag{11}$$

$$f_1\left(\frac{\kappa_p}{\kappa_0}\right) = 1 - \frac{\kappa_p}{\kappa_0} \tag{12}$$

$$f_2\left(\frac{\rho_p}{\rho_0}, \frac{2\delta}{d}\right) = \Re\left[\frac{2\left[1-\gamma\left(\frac{2\delta}{d}\right)\right]\left(\frac{\rho_p}{\rho_0}-1\right)}{2\frac{\rho_p}{\rho_0}+1-3\gamma\left(\frac{2\delta}{d}\right)}\right] \tag{13}$$

$$\gamma\left(\frac{2\delta}{d}\right) = -\frac{3}{2}\left[1 + i\left(1 + \frac{2\delta}{d}\right)\right]\frac{2\delta}{d} \tag{14}$$

where E_{ac} is the acoustic energy density, d is the diameter of the particle or drop, z is the distance from the transducer along the central axis in the ultrasonic standing wave field, $k = n\pi/h$, n is the number of half wavelengths between the acoustic transducer and the reflector, h is the distance between the transducer and the reflector, ρ_p is the density of the particle or drop, ρ_0 is the density of air, κ_p is the compressibility of the particle or drop, κ_0 is the compressibility of air, and δ is the thickness of the acoustic boundary layer (Eq. (9)). Figure 17 is a plot of F_{ar} for a PSL particle, as a function of d. In this plot, the $\sin(2kz)$ portion of Eq. (10) is set to unity, so we are plotting F_{ar} at the z location where it is a maximum. The theories of Settnes & Bruus (2012), Doinikov (1997), Danilov & Mironov (2000), and the inviscid theory of King (1934), are also included for completeness in this figure. The gap in Doinikov's theory in Fig. 17 is due to the fact that this theory only applies to conditions where the particle size is much larger or much smaller than the characteristic lengths for momentum transfer and conduction around the oscillating particle. The discontinuity around 3 μm in Danilov's theory is due to the fact that the plot of F_{ar} versus d changes sign at this diameter, which cannot be displayed on a log–log plot. Doinikov's theory also predicts a change in sign of the force on the particle when going from the low diameter to the high diameter range of his theory (Doinikov, 1997). The Settnes & Bruus (2012) theory does not exhibit a sign change. Note that as F_{ar} is plotted here, a sign change signifies that particles would change their stable location from a node to an anti-node, or vice versa.

Values for all of the variables in Eqs. (10)–(14) are easily obtained except for E_{ac}, which is difficult to measure. Accordingly, to obtain numerical values for F_{ar} in Fig. 17, we used our current transducer as an example, and set the applied

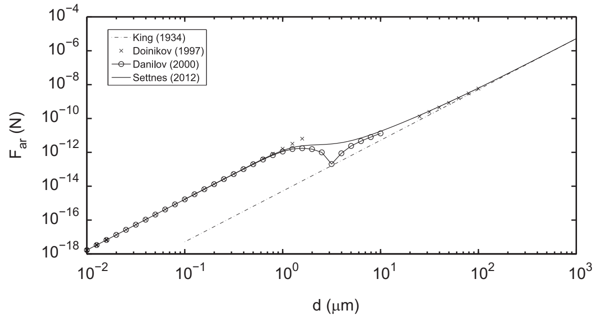

Fig. 17. Acoustic radiation force predicted by various theories. The plot is for an ultrasonic frequency of 30 kHz, a PSL particle, and for air as the surrounding gas.

voltage to the typically used value. Then we levitated a water drop in the field, ascertained its diameter via a camera with a known pixels/mm calibration and then slowly decreased the voltage until the drop fell. We then set the weight of the drop equal to F_{ar} in Eq. (10), using properties for water in all of the relevant parameters. This enabled us to extract a value for E_{ac}. Assuming that E_{ac} is not a function of the properties of the drop or particle in the field we then used this value of E_{ac} to obtain plots for F_{ar} for particles and drops, etc.

Figure 17 shows that all three viscous theories exhibit reasonable agreement for $d > 100\ \mu m$, where the theory is well-studied and where experimental data has been obtained and used to validate the theories (Baer et al., 2011). However, for the diameter range of interest here, $0.1\ \mu m < d < 10\ \mu m$, these theories deviate significantly from each other in magnitude and sign; moreover, experimental studies have not been conducted to validate any of the viscous theories presented in Fig. 17. Accordingly, as noted above, we will focus on the theory of Settnes & Bruus (2012) for convenience, since it is continuous over the diameter range of interest.

As noted above, we hypothesize that the increase in scavenging which we have observed in the presence of an ultrasonic standing wave field is due to the following: (1) an increase in particles combining with each other, (2) an increase in particles combining with small drops, or (3) an increase in particles combining with big drops. A combination of these three could also occur. Here, small drops refer to drops generated by the nebulizer that have not agglomerated, and large drops refer to the millimeter-scale drops seen in the center of the accretion disks (see Fig. 2), formed by the agglomeration of small drops.

To help determine which of the above is occurring, we take advantage of the fact that there is a finite air velocity of ~ 2 cm/s in our apparatus which carries the particles into the chamber. This velocity was obtained by dividing the volumetric flow rate of air through the scavenging chamber by the cross-sectional area of the box perpendicular to the air flow direction. This velocity will result in a drag force on any particle or drop that may be held in place by F_{ar}. If $F_d > F_{ar}$, then it is unlikely that the acoustic radiation force will have a significant impact on the particle or drop. Figure 18 plots both F_{ar} and F_d against d, where F_d is obtained for a velocity of 2 cm/s using a drag coefficient versus Reynolds number relation for a perfect sphere (Crowe et al., 2009), and F_{ar} is obtained using the value of E_{ac} obtained as described above. The figure shows that the two plots cross over at $d = 17\ \mu m$, meaning that $F_{ar} > F_d$ for $d > 17\ \mu m$. This indicates that F_{ar} has little direct impact on the micron-scale particles investigated in this work, since the air flow will have greater impact on micron scale particles than the acoustic radiation force. However, the fine water drops in the spray used here (order of 100 μm in diameter), as well as the large drops that accumulate in the center of the accretion disks (order of millimeters in diameter), all experience a larger force due to the ultrasonics than the air flow. Hence, if the theory of Settnes & Bruus (2012) is correct, then the increase in scavenging that we have observed is not due to the ultrasonics directly moving particles into the accretion disks. Most likely, what is occurring is that the large number of fine water drops, which are significantly influenced by the ultrasonics, are entrained into the accretion disks and entrain particles in their wake. Once in the accretion disks, the number density of both particles and drops has increased, thereby increasing the chance for particle scavenging. Of course the above assumes that the theory of Settnes & Bruus (2012) is correct in both its functional forms, and in the absolute value of F_{ar}.

An exciting aspect of Fig. 18 is that it suggests that particles could be directly affected by F_{ar}, if sufficient power is provided to the transducer. In other words, if enough power was provided to the transducer so that the crossover point $F_{ar} = F_d$ occurs at a diameter of a micron, then particle accretion disks would form in the ultrasonic standing wave field for micron-scale particles, independent of whether drops were present or not. The inclusion of drops would only further enhance scavenging. Moreover, because the value of d at which $F_{ar} = F_d$ can be controlled by the magnitude of F_{ar} and hence by power to the transducer, this cutoff diameter is easily controlled, enabling selective scavenging of particles greater than a selected diameter.

It is possible that some of what is observed here may be due to acoustic streaming, the process whereby a fluid flow is created by an acoustic field due to the dissipation of the acoustic energy by the fluid. It is unlikely that acoustic streaming

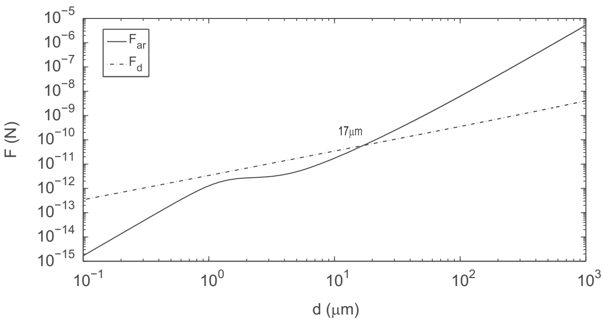

Fig. 18. Comparison of the acoustic radiation force F_{ar} with the aerodynamic drag force F_d acting on a particle of diameter d. The acoustic radiation force is obtained from the theory of Settnes & Bruus (2012). We use this figure in the discussion of both PSL particles and water drops, though the properties of water are used to obtain the plot. This is acceptable since, on the scale of this plot, using PSL properties results in a plot that is indistinguishable from that presented here.

could account for the levitation of the millimeter scale drops observed in the center of the accretion disks (Fig. 2). In order for this to be the case, the upward directed streaming velocity would have to be equal to the terminal velocity of the largest levitated drop, which would be about 7 m/s (Beard & Pruppacher, 1969; Berry & Pranger, 1974; Foote & DuToit, 1969; Gunn & Kinzer, 1949). Visual observation of the velocities at which the fine water drops moved about in the standing wave field was nowhere near this value, having velocities on the order of a centimeter per second. Moreover, according to the theory of acoustic streaming developed by Lighthill (1978), a velocity of 7 m/s would have required an acoustic power two orders of magnitude larger than that which was actually applied to the transducer in our setup. Accordingly, it is clearly the acoustic radiation force which is responsible for the levitation of the large drops. However, experimental studies of streaming have shown that in experimental setups similar to that used here, streaming velocities on the order of a centimeter per second can be achieved (Rednikov et al., 2006; Trinh & Robey, 1994). These velocities are on the order of the airflow velocities in the present work, and so it is possible that streaming did influence the overall flow field in this work, and thereby the paths of the particles and small drops. However, in the work cited above, these flows create structures that are comparable to the size of the transducer as well as vortex shedding near the container walls or from a large drop. It is unlikely, therefore, that streaming could account for the fine-scaled accretion disk structure seen in Fig. 2 though, again, it could have some effect on the overall fluid flow and thereby on the scavenging behavior. Further work is needed to quantify the effect of streaming on the scavenging coefficient.

5. Conclusion

The experimental work presented herein demonstrated that the combination of a water spray with an ultrasonic standing wave field can significantly improve the scavenging of micron-scale particles. For the conditions studied here, particle scavenging was improved by as much as 150% using ultrasonics with water sprays, when compared to using water sprays alone. Accretion disks were observed to form in the pressure nodes of the standing wave field and it was shown that these were critical to the improved particle scavenging observed in the presence of ultrasonics. Invoking the theory of the ultrasonic radiation force F_{ar}, it was demonstrated that it is unlikely that the observed improvements in scavenging were due to direct action by F_{ar} on the particles. Rather, it is more likely that F_{ar} acts on the water droplets, and that these droplets entrain particles in their wake, concentrating both particles and drops in the accretion disks and thereby increasing particle scavenging.

Acknowledgments

This work was partially funded by NIOSH and NSF whose support is gratefully acknowledged.

References

Baer, S., Andrade, M.A., Esen, C., Adamowski, J.C., Schweiger, G., & Ostendorf, A. (2011). Analysis of the particle stability in a new designed ultrasonic levitation device. *Review of Scientific Instruments*, *82*, 105111–105117.

Beard, K.V. (1974). Experimental and numerical collision efficiencies for submicron particles scavenged by small raindrops. *Journal of the Atmospheric Sciences*, *31*(6), 1595–1603.

Beard, K.V., & Grover, S.N. (1974). Numerical collision efficiencies for small raindrops colliding with micron size particles. *Journal of the Atmospheric Sciences*, *31*(2), 543–550.

Beard, K.V., & Pruppacher, H.R. (1969). A determination of the terminal velocity and drag of small water drops by means of a wind tunnel. *Journal of the Atmospheric Sciences*, *26*, 1066–1072.

Berry, E.X., & Pranger, M.R. (1974). Equations for calculating the terminal velocities of water drops. *Journal of Applied Meteorology*, *13*, 108–113.

Cohen, A.J. (2000). Outdoor air pollution and lung cancer. *Environmental Health Perspectives*, *108*, 743–750.

Crowe, C.T., Elger, D.F., Williams, B.C., & Roberson, J.A. (2009). *Engineering fluid mechanics*. John Wiley & Sons: .

Crum, L.A. (1971). Acoustic force on a liquid droplet in an acoustic stationary wave. *Journal of the Acoustical Society of America*, *50*, 157–163.

Danilov, S.D., & Mironov, M.A. (2000). Mean force on a small sphere in a sound field in a viscous fluid. *Journal of the Acoustical Society of America*, *107*, 143–153.

Davis, D.L., Bell, M.L., & Fletcher, T. (2002). A look back at the London smog of 1952 and the half century since. *Environmental Health Perspectives*, *110*, A734–A735.

Dockery, D.W., & Pope, C.A. (1994). Acute respiratory effects of particulate air pollution. *Annual Review Public Health*, *15*, 107–132.

Doinikov, A.A. (1997). Acoustic radiation force on a spherical particle in a viscous heat-conducting fluid. I. General formula. *Journal of the Acoustical Society of America*, *101*, 713–721.

EPA (1999). *Air quality criteria for particulate matter* (Vol. II). Technical Report EPA document 600/P-99/002b EPA.

Foote, G.B., & DuToit, P.S. (1969). Terminal velocity of raindrops aloft. *Journal of Applied Meteorology*, *8*, 249–253.

Gor'Kov, L.P. (1962). On the forces acting on a small particle in an acoustical field in an ideal fluid. *Soviet Physics Doklady*, *6*, 773–775.

Greenfield, S.M. (1957). Rain scavenging of radioactive particulate matter from the atmosphere. *Journal of Meteorology*, *14*, 115–125.

Gunn, R., & Kinzer, G.D. (1949). The terminal velocity of fall for water droplets in stagnant air. *Journal of Meteorology*, *6*, 243–248.

Hasegawa, T., & Yosioka, K. (1969). Acoustic-radiation force on a solid elastic sphere. *Journal of the Acoustical Society of America*, *46*, 1139–1143.

Heyder, J., Gebhart, J., Rudolf, G., Schiller, C.F., & Stahlhofen, W. (1986). Deposition of particles in the human respiratory tract in the size range 0.005–15 μm. *Journal of Aerosol Science*, *17*, 811–825.

Johnson, R.L. (2004). Relative effects of air pollution on lungs and heart. *Circulation*, *109*, 5–7.

King, L.V. (1934). On the acoustic radiation pressure on spheres. *Proceedings of the Royal Society of London. Series A – Mathematical and Physical Sciences*, *147*, 212–240.

Lighthill, S.J. (1978). Acoustic streaming. *Journal of Sound and Vibration*, *61*, 391–418.

Marston, P.L., & Thiessen, D.B. (2004). Manipulation of fluid objects with acoustic radiation pressure. *Annals of the New York Academy of Sciences*, *1027*, 414–434.

NIOSH (2002). *Work-related lung disease surveillance report* 2002. Technical Report NIOSH Publication No. 2003-111 NIOSH.

Ostu, N. (1979). A threshold selection method from gray-level histogram. *IEEE Transactions on Systems, Man, and Cybernetics*, *9*, 62–66.

Pope, C.A., Burnett, R.T., Thun, M.J., Calle, E.E., Krewski, D., Ito, K., & Thurston, G.D. (2002). Lung cancer, cardiopulmonary mortality, and long-term exposure to fine particulate air pollution. *Journal of the American Medical Association*, *287*, 1132–1141.

Pope, C.A., Burnett, R.T., Thurston, G.D., Thun, M.J., Calle, E.E., Krewski, D., & Godleski, J.J. (2004). Cardiovascular mortality and long-term exposure to particulate air pollution. *Circulation*, *109*, 71–77.

Pope, C.A., Thun, M.J., Namboodiri, M.M., Dockery, D.W., Evans, J.S., Speizer, F.E., & Heath, C.W. (1995). Particulate air pollution as a predictor of mortality in a prospective study of U.S. adults. *American Journal of Respiratory and Critical Care Medicine*, *151*, 669–674.

Pranesha, T.S., & Kamra, A.K. (1996). Scavenging of aerosol particles by large water drops: 1. Neutral case. *Journal of Geophysical Research*, *101*, 23373–23380.

Rednikov, A.Y., Zhao, H., Sadhal, S.S., & Trinh, E.H. (2006). Steady streaming around a spherical drop displaced from the velocity antinode in an acoustic levitation field. *Quarterly Journal of Mechanics and Applied Mathematics*, *59*, 377–397.

Santesson, S., & Nilsson, S. (2004). Airborne chemistry: Acoustic levitation in chemical analysis. *Analytical and Bioanalytical Chemistry*, *378*, 1704–1709.

Schikowski, T., Sugiri, D., Ranft, U., Gehring, U., Heinrich, J., Wichmann, H.-E., & Kramer, U. (2005). Long-term air pollution exposure and living close to busy roads are associated with COPD in women. *Respiratory Research*, *6*, 152.

Schwartz, J. (1994). What are people dying of on high air pollution days?. *Environmental Research*, *64*, 26–35.

Schwartz, J., & Dockery, D.W. (1992). Increased mortality in Philadelphia associated with daily air pollution concentrations. *American Review of Respiratory Disease*, *145*, 600–604.

Schwartz, J., Laden, F., & Zanobetti, A. (2002). The concentration-response relation between PM2.5 and daily deaths. *Environmental Health Perspectives*, *110*, 1025–1029.

Schwartz, J., Slater, D., Larson, T.V., Pierson, W.E., & Koenig, J.Q. (1993). Particulate air pollution and hospital emergency room visits for asthma in Seattle. *American Review of Respiratory Disease*, *147*, 826–831.

Seaton, A., Godden, D., MacNee, W., & Donaldson, K. (1995). Particulate air pollution and acute health effects. *Lancet*, *345*, 176–178.

Settnes, M., & Bruus, H. (2012). Forces acting on a small particle in an acoustical field in a viscous fluid. *Physical Review E*, *85*, 016327.

Shi, W.T., Apfel, R.E., & Holt, R.G. (1996). Instability of a deformed liquid drop in an acoustic field. *Physics of Fluids*, *7*, 2601–2607.

Suwa, T., Hogg, J.C., Quinlan, K.B., Ohgami, A., Vincent, R., & van Eeden, S.F. (2002). Particulate air pollution induces progression of atherosclerosis. *Journal of the American College of Cardiology*, *39*, 935–942.

Tang, I.N. (1976). Phase transformation and growth of particles composed of mixed salts. *Journal of Aerosol Science*, *7*, 361–371.

Trinh, E.H. (1985). Compact acoustic levitation device for studies in fluid dynamics and material science in the laboratory and microgravity. *Review of Scientific Instruments*, *56*, 2059–2065.

Trinh, E.H., Holt, R.G., & Thiessen, D.B. (1996). The dynamics of ultrasonically levitated drops in an electric field. *Physics of Fluids*, *8*, 43–61.

Trinh, E.H., & Robey, J.L. (1994). Experimental study of streaming flows associated with ultrasonic levitators. *Physics of Fluids*, *6*, 3567–3579.

Verrier, R.L., Mittleman, M.A., & Stone, P.H. (2002). Air pollution: An insidious and pervasive component of cardiac risk. *Circulation*, *106*, 890–892.

Weber, J.K., Hampton, D.S., Merkley, D.R., Rey, C.A., Zatarski, M.M., & Nordine, P.C. (1994). Aero-acoustic levitation: A method for containerless liquid-phase processing at high temperatures. *Review of Scientific Instruments*, *65*, 456–465.

Whitby, K.T., & Liu, Y.H. (1968). Polystyrene aerosols-electrical charge and residue size distribution. *Atmospheric Environment*, *2*, 103–116.